SASSPR: Semi-Automated Sensor for Surface Plasmon Resonance

Robin Howell, Robert Ballentine, James Henderson

Dept. of Electrical and Computer Engineering, College of Optics and Photonics, University of Central Florida, Orlando, Florida, 32816-2450

***Abstract* — We present a low-cost surface plasmon resonance (SPR) sensor using the Kretschmann configuration. Our device will observe the optical phenomenon called surface plasmon excitation, which is created by directing a laser of 635 nm at a particular incidence angle onto a prism with gold film attached to one surface. At this particular angle, phase matching can occur between the wave of the incident light and that of the surface plasmons. The transfer of energy from the photons to the surface plasmons leads to a significant drop in intensity of the reflected beam, which is detected using a CMOS sensor camera. A software application is used to display in a graphical format the changes seen when excitation occurs as well as the shift in the surface plasmon resonance angle when the dielectric material at the gold film interface changes from a low refractive index to a higher refractive index, thus demonstrating how the device would work for monitoring molecular binding in an experimental setting.**

***Index Terms* — Surface Plasmon Resonance, Laser Diode Module, CMOS Sensor Detector, Embedded Software.**

I. Introduction

In drug development, pre-clinical trials are the first step for drug discovery. During this step, information such as the safety, dosage, and metabolism of the drug are determined before any human clinical trials are performed. To do this, biosensing instruments such as Surface Plasmon Resonance (SPR) sensors are used to determine these various factors by observing binding interactions among molecules using label-free detection methods. However, commercial Surface Plasmon Resonance sensors can be very costly, with an average range of $40,000, making it difficult for many biochemistry labs to obtain this accurate biosensing instrument.

The device being developed is a low-cost, intensity modulation Kretschmann geometry based surface plasmon resonance sensor. The primary functions of the device are a right-angled prism and a 50 nm thin gold film. Kretschmann geometry utilizes the process of total internal reflection and the reflectivity value of the light to measure the excitation of surface plasmon polaritons on the surface of the gold film when the incident wave of a light source is properly phase matched with the wave of the surface plasmons on the metal-dielectric interface. The device will operate under two conditions: one with the gold film in air, and the other will consist of the gold film being submerged in distilled water. Adding the distilled water will result in the refractive index of the dielectric material on contact with the gold surface to change, which leads to a shift in the resonance angle where surface plasmon excitation occurs. Doing so will provide us with information on how the surface plasmon resonance sensor would monitor molecular binding using intensity modulation should this experiment continue beyond what is currently presented.

II. Design Description

Our device will detect when excitation of surface plasmons occur and monitor shifts in the surface plasmon resonance angle when changes to the metal-dielectric interface take place. This will be done using an optical setup that detects the surface plasmon interactions through changes in the light source's intensity. The hardware components include a laser diode module, a polarizing beamsplitter, a motorized rotation stage, a N-BK7 uncoated right-angle prism, a gold surface plasmon resonance (SPR) chip, a CMOS sensor camera, and a microcontroller unit. The change in intensity is monitored using the CMOS sensor camera that is controlled using the microcontroller unit. The captured images from the camera will be transmitted via Wi-Fi to a compatible device where the detectable information will be extrapolated and displayed through a self-developed software application. The application will extract the intensity profile of each captured image and provide a graphical representation of the intensity changes observed over time. A collimated 635 nm laser diode module was chosen as the light source for this experiment. The beam undergoes slight modifications before the light propagates through the prism and interacts with the gold chip attached to its surface. A polarizing beamsplitter is used to allow only p-polarized light be transmitted through the optical system to ensure that phase matching will occur between the incident light wave and the wave of the surface plasmons. The light is directed onto the right-angle prism that is placed onto a motorized rotation stage. A gold SPR chip is attached to the prism using index matching gel with a refractive index of 1.5 to match the refractive index of the N-BK7 glass right-angle prism and minimize

refraction of our light before interaction with the gold film. Due to total internal reflection from the right-angle prism, the incident light deviates 90 degrees and exits the prism from the opposite leg. The CMOS sensor camera is placed directly after the light exits the prism to capture its intensity values for further evaluation. The right-angle prism is mounted into a 3D printed casing containing a sensor chamber where liquid can be added to observe how changes from a low refractive index medium, air, to a higher refractive index medium, liquids, shifts the resonance angle where surface plasmon excitation can occur. The entire setup is enclosed in a housing unit made of black polyethylene to minimize external light affecting the final results as well as provide safety from the collimated beam emitting from the laser diode module that could result in eye damage. Figure 1 provides an illustration of the final design for our device.

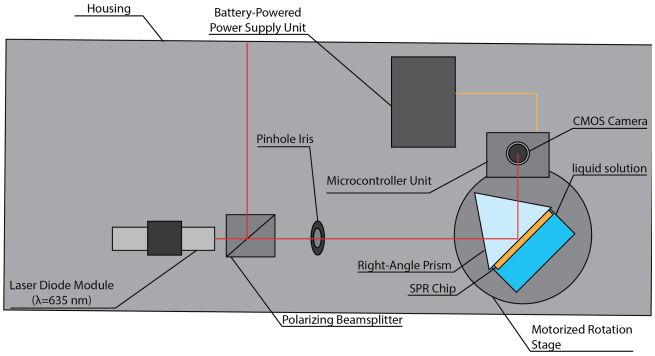

Figure 1. Schematic diagram of Semi-Automated Sensor for Surface Plasmon Resonance.

To begin the experiment, the user powers on the laser diode module using a wall-plug power cable and turns on the motorized rotation stage using the K-Cube DC Servo Motor Controller provided by Thorlabs. This controller is required to connect directly to the motorized rotation stage due to Kinesis, the software package included with the rotation stage, is a closed-source software which minimized how much automation we could provide to the motorized rotation stage. The user rotates the stage from a range of 44-48° at a velocity of 0.5° per second and an acceleration of 2° per second. The velocity and acceleration were chosen to ensure that the prism is rotated at a slow enough speed so the camera can properly detect the intensity changes observed from the reflected light off of the prism. The software application created for this product is turned on using a Windows computer. The software controls the CMOS sensor camera's power and various settings and therefore is used to instruct the camera to begin capturing 1 image every 0.5 seconds and processing the intensity profile of the uploaded images to display graphically to the user. Once the user has increased the angle to greater than the critical angle, excitation of the surface plasmons can occur when the angle is precise for phase matching between the incident wave of light and the wave of the surface plasmons. This excitation is represented by a significant drop in the reflected light's intensity on the detector. The drop in intensity will be displayed on the graph provided by the software application, as well as in a numerical format, showing the intensity changes over time.

Once the resonance angle for surface plasmon excitation in air is determined, the user will then add a liquid into the sensor chamber and monitor any changes in the intensity of the reflected light onto the CMOS sensor camera. An increase in the intensity correlates with a shift in the resonance angle, due to a change in the refractive index of the material interacting with the surface of the gold film. This is a form of surface plasmon resonance sensing called intensity modulation, where the angle of incidence remains fixed and an increase in light intensity is observed by the detector when the angle for surface plasmon resonance changes. Therefore, our device informs the user of when in time surface plasmon resonance occurred, how well the photons coupled to the surface plasmons through the measured dip in light intensity, and if a shift in the resonance angle was observed when changing the refractive index of the dielectric material at the interface between the gold film.

III. Hardware Design Components

A. Laser Diode Module

For our device, we have chosen a 635 nm wavelength laser diode module with a beam divergence of 0.6 mrad from Thorlabs. The laser emits an output power of 1.2 mW, which was chosen to avoid large laser output power that could be dangerous when in use. For our purposes, large output optical power is not required for surface plasmon excitation to occur. The chosen wavelength for our laser diode was determined after various simulations and calculations were performed. A 532 nm and a 635 nm laser diode were compared theoretically to observe how longer wavelengths would affect our final experiment when compared to shorter wavelengths. Figure 2 shows a simulation of surface plasmon resonance curves for the two wavelengths in question using only p-polarized light.

Wavelength (nm)	Real Part of Dielectric Function of 50nm Gold, ε'1	Imaginary Part of Dielectric Function of 50nm Gold, ε''1	Length of Intensity Decay Along Direction of Propagation, L (μm)	Phase Velocity, v_p/c
532	-4.0	1.3	0.677	0.866
635	-8.0	0.9	5.88	0.935

Table 1. Calculated parameters characterizing propagation of SP on metal-air interface.

The simulation was created using Winspall, a free software for simulating surface plasmon resonance curves based on the Fresnel formalism. As can be seen, the 532 nm laser has a broader peak compared to that of the 635 nm laser. The reason for this broad peak observed was investigated by estimating the real and imaginary parts of the dielectric function as a function of wavelength of the gold film and calculating the length of intensity decay of the surface plasmons along the length of propagation and their phase velocity. The calculated values can be seen in Table 1. The real and imaginary parts of the gold film dielectric function were determined by using known real and imaginary values for typical 50 nm gold film and later fitted using the software Winspall until the resonance curves matched known resonance curves of similar wavelengths. The final estimated values are supported by the fact that the absolute value of the imaginary part of the dielectric function decreases as the wavelength increases, as is to be expected due to the relation of wavelength with the dielectric function of the metal [1].

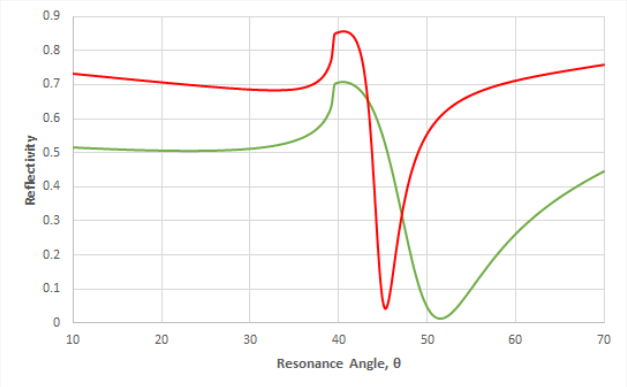

Figure 2. Simulated surface plasmon resonance curve for two distinct wavelengths: 532 nm (green) and 635 nm (red).

The fluctuations created by the electron charges on a metal boundary are called surface plasmon oscillations. The charge fluctuations contain a transverse and longitudinal electromagnetic field which disappears as $|z| \rightarrow \infty$, with a maximum on the surface at z = 0 [2]. The field is given by

$$E = E_0^{\pm} \exp\left[+i(k_x x \pm k_z z - \omega t)\right], \quad (1)$$

with + for z ≥ 0, - for z ≤ 0, and the imaginary k(z) leading to an exponential decay of the field E(z). Using Maxwell's equations, the retarded dispersion relation for the plane surface of a semi-infinite metal with the dielectric function (ε1 = ε'1 + iε''1) next to a medium such as air, denoted by ε2, is given as

$$D_0 = \frac{k_{z1}}{\varepsilon_1} + \frac{k_{z2}}{\varepsilon_2} = 0, \quad (2)$$

along with

$$\varepsilon_i \left(\frac{\omega}{c}\right)^2 = k_x^2 + k_{zi}^2 \quad (3)$$

or

$$k_{zi} = \left[\varepsilon_i \left(\frac{\omega}{c}\right)^2 - k_x^2\right]^{1/2}, \quad i = 1, 2. \quad (4)$$

The dispersion relation in Equation (2) can then be rewritten for the transverse components of the surface plasmon wave vector as

$$k_x = \frac{\omega}{c}\left(\frac{\varepsilon_1 \varepsilon_2}{\varepsilon_1 + \varepsilon_2}\right)^{1/2}, \quad (5)$$

with ε1 relating to the dielectric function of the metal and ε2 relating to the dielectric function of the medium adjacent to it. The real part of the complex wave vector can be written as

$$k_x' = \frac{\omega}{c}\left(\frac{\epsilon_1' \epsilon_2}{\epsilon_1' + \epsilon_2}\right)^{1/2}, \quad (6)$$

while the imaginary part of the complex wave vector is given by

$$k_x'' = \frac{\omega}{c}\left(\frac{\epsilon_1'\epsilon_2}{\epsilon_1' + \epsilon_2}\right)^{3/2} \frac{\epsilon_1''}{2(\epsilon_1')^2}. \quad (7)$$

Surface plasmons decay along the direction of propagation until their energy is lost due to absorption in the metal interface or scattering into free space [2]. The length of this intensity decay can be calculated using

$$L = \frac{1}{2k_x''}. \quad (8)$$

As can be seen, the length of decay is inversely related to the imaginary part of the complex wave vector. At higher frequencies, the mode diameter is smaller [1], which leads to more light on the metal surface. The metal absorbs the light and increased mode overlap is observed, leading to an increase in dissipation. This increase in dissipation leads to a decrease in the amplitude of oscillation, known as damping [1]. From the estimated imaginary parts of our complex dielectric function, it can be observed that shorter wavelengths will have stronger damping in comparison to longer wavelengths. The imaginary part of the complex wave vector therefore plays a role in the internal absorption of the metal. Equations (6) and (7) were used to calculate the real and imaginary parts of the complex wave vector and were subsequently used to calculate their respective length of decay. From the calculated parameters, it was observed that as the imaginary part of the complex wave vector decreases, as was seen for longer wavelengths, the length of intensity decay increases.

The phase velocity of the surface plasmons was another parameter to investigate, with can be calculated using

$$v_p = \frac{\omega}{k_x'}. \quad (9)$$

Comparing the phase velocity of the two wavelengths, it is clear that the velocity increases with longer wavelengths. Light slows down when coupled to a plasmon [1], but it can be concluded from our calculations that the phase velocity is slower for shorter wavelengths when compared to longer wavelengths. The decrease in phase velocity, alongside the strong damping observed by shorter wavelengths, leads to a noticeable broadening of the resonance curve. The broadening informs us how quickly over a distance the modes lose their amplitude [1]. Therefore, to generate a surface plasmon resonance curve with a distinct angle where a drop in intensity is observed, longer wavelength lasers are required. Due to this, a 635 nm wavelength light source was a preferred choice for our surface plasmon resonance sensor.

B. Polarizing Beamsplitter

It is important that the light used to excite the wave of the surface plasmons on the gold film is parallel polarized, or p-polarized, to ensure phase matching of the k-vectors between the light's incident wave and the surface plasmon wave can occur. A polarizing beamsplitter from Thorlabs was chosen to ensure that only p-polarized light is transmitted through the optical system, and s-polarized light is reflected and directed onto a beam blocker. The polarizing beamsplitter contains a dielectric coating along the diagonal interface between two right-angle prisms cemented together to create a cube shape. The coating ensures that s-polarized light is reflected and p-polarized light is transmitted, with an extinction ratio for transmitted light of T_P:T_S > 1000:1.

C. Right-Angle Prism

The method for coupling the incident light wave to that of the surface plasmons was done with a N-BK7 right-angle prism. The prism was chosen due to it's inexpensive pricing and the ease of upkeep. This material holds a refractive index value of 1.52 and has a transmission value of 93% using a 635 nm wavelength. This is important because the critical angle of the prism can be determined theoretically for testing purposes using

$$\theta_{crit} = \sin^{-1}(n_r/n_i), \quad (8)$$

where n(i) is the refractive index of the prism and n(r) is the refractive index of air, 1. Using the equation, it can be found that the critical angle of the prism is around 41°, where angles greater than this will observe total internal reflection. The dimensions of the prism are 20mm x 20mm x 20mm. Having a larger prism allows for less restrictions on movement as the beam has more travel as it impinges on the face of the prism.

D. Surface Plasmon Resonance Sensor Chip

Our project focuses around the excitation of the surface plasmons at the gold-dielectric interface. Commonly, the metal film is deposited on one side of a very thin glass slide where the glass surface is pressed against the prism. The thickness of the film itself is a crucial component to consider for excitation of the surface plasmons to occur. Figure 3 illustrates the reflectivity of various thicknesses of silver film at a constant wavelength using attenuated total internal reflection. Although this example is utilizing silver instead of gold, it nevertheless informs us of the

varying reflection observed at different thicknesses. Energy conservation requires that

$$R + A + T = 1 , \quad (9)$$

which relates to the summation of the relative reflection, absorption, and transmission, respectively [2]. The incident light wave is partially reflected at the interface. It partially transverses the metal film as an exponentially decaying wave. At half the interface, it induces excitation which in turn radiates light back into the metal film [2]. For thicknesses smaller than 490 Å, the back scattered field increases. Since it is in antiphase with the incoming light wave, the two destructively interfere which reduces R. Since transmission, T, equals 0, and at the minimum thickness, d(min), R = 0, A subsequently becomes 1. This leads to all of the energy being absorbed into the metal film and can be noted in Figure 3 by the reflection observed at 290 Å film thickness. For thicknesses larger than 490 Å, the back scattered field disappears so that R approaches close to the value unity, 1. Thus, absorption in the metal film is not greatly observed which leads to a small and narrow dip in reflection as can be seen for the film thickness 890 Å in Figure 3.

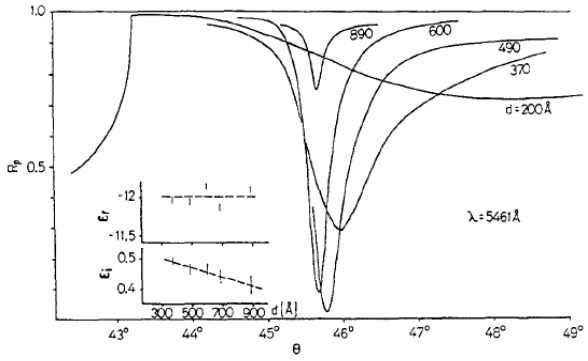

Figure 3. Reflection observed on silver film at varying thicknesses measured using attenuated total internal reflection.

Therefore, it can be concluded that for proper excitation of the surface plasmons to occur, the metal should have a film thickness of about 490 Å, or 49 nm. Manufactured glass slides with the proper film thickness deposited are available for consumer purchase, commonly known as surface plasmon resonance (SPR) sensor chips. The chips purchased for this experiment are from the company Sofchip, which provided 20 x 20 mm bare gold chips with a film thickness of 50 nm. The chips were chosen due to the ease of use for the experiment, allowing us to avoid depositing 50 nm in diameter gold nanoparticles onto a microscope slide ourselves which could have led to an uneven surface and potential errors in our final calculations. It should be noted, however, that the SPR chips cannot be reused indefinitely and wear and tear was observed on each chip after multiple uses in experiments, especially when submerged in the liquid solution. Therefore, our device contains a parameter where constant purchase of gold SPR chips is required in order to use the device. This parameter cannot be avoided, as it is a feature of all surface plasmon resonance sensors.

E. CMOS Sensor Camera

Our priorities when selecting a camera sensor were compatibility and quality. The compatibility of the sensor was most important since we are basing our predictions off an experiment that uses a mobile phone's camera as the image sensor. The OV2640 was selected since it has a history of use in Android and Apple mobile devices while still going strong to this day. A high capture rate of the image sensor is important to ensure a smooth and continuous change in the data when detecting SPR. The sensor must be sensitive enough to measure the potentially small yet significant change in intensity when SPR occurs.

The OV2640 supports a resolution up to 1600 x 1200 with a capture rate up to 15 frames per second at that resolution. With the onboard JPEG compression, low latency uploads will be very easy on low-end ARM microprocessors. The engineering requirement for our device is to capture an image twice a second with a significant enough resolution for an accurately perceived brightness detection which the OV2640 is more than capable of.

F. Microcontroller

The responsibility of the microcontroller has experienced many changes throughout the development of the SPR device. The final version of the system required the microcontroller to host a webserver that would allow control over the image sensor to be given to the client software. The microcontroller needs to maintain a consistent capture rate to ensure accurate data collection.

Table 2 shows the results of testing the capture rate against the clock rate and pixel resolution to ensure we can fulfil our engineering requirement of 2 images per second with a high enough resolution to ensure accurate data interpretation. The latency of the processing time is not as important as the upload latency but neither value will negatively affect our engineering requirements if the application can account for them when measuring the incoming data.

Many different microcontrollers would fit well into this experiment but the chosen one, the ESP32-CAM, was chosen for its extremely low cost, low energy consumption, and the newly developed parallel camera installed in the original ESP32.

Clock Rate	Pixel Resolution	Captures/seconds	Average Processing Time	Max/Min Processing Time
240 MHz	1600 x 1200	12.2	79 ms	209 ms/73 ms
240 MHz	800 x 600	25.6	40 ms	61 ms/38 ms
160 MHz	1600 x 1200	11.9	83 ms	162 ms/74 ms
160 MHz	800 x 600	27.1	39 ms	98 ms/42 ms
80 MHz	1600 x 1200	8.3	112 ms	185 ms/67 ms
80 MHz	800 x 600	25.6	39 ms	72 ms/34 ms

Table 2. ESP32-CAM Capture vs. Clock Frequency

G. 3D Printed Components

Designing a consumer-grade tool requires a specially designed form-fitting case to conceal the hardware and optics equipment. To ensure the internal components are well protected yet still serviceable, custom 3D printed housings and mounts were designed in photopolymer resin for nonporous purposes and thermoplastics for general use.

All models were developed in AutoDesk's Fusion360 to ensure the least amount of distortion when converting the 3D models into printable file types that the printing software will use to generate the preparatory codes. This can be a real issue when 3D printing such small models that require highly accurate tolerances. The glass prism is very sensitive to pressure and prone to scratches. When designing the container that would house the fluid behind the gold chip, the tolerance issues will become most noticeable. We do not want to break the prism between experiments but the fluid can leak out the corners of the prism if there is enough room. We experimented with silicone o-rings and scrap rubber but due to time constraints our final version of the SPR device has the prism permanently locked into the container using hot glue. This will assure a water-tight container without damaging the glass prism as alcohol can greatly weaken the hot glue and allow easy removal with little to no remaining residue.

With the original design of our SPR device, we wanted a fully portable product and 3D printing was a necessity to create such a form fitting case and housing. There are several 3D prints in the final version of our product but the most important are the electronics housing the more complex prism container that also mounts the microcontroller and holds the liquid for the experiment. Figure 4 illustrates the final rendering of the prism container and the ESP mount.

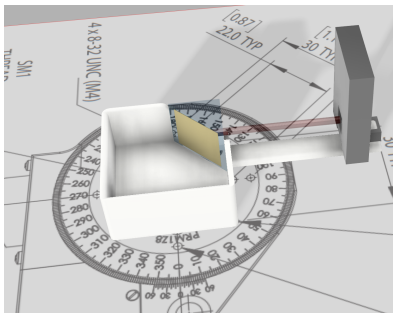

Figure 4. Rendering of Prism Container and ESP Mount

H. Power Supply

The power supply for the SPR device had originally been designed to power the laser diode and microcontroller unit and share the circuit board space with the transistor logic that would control the flow of power to the laser diode for an automated control during the experiment. The power supply would accept an input from a 7.4v LiPo battery and house the charging circuit for the battery. At any time, the AC wall adaptor can be connected as an input and the flow of power from the battery will stop to ensure a constant supply of power to the experiment for portable use.

The final design for the SPR device still houses the hardware to fulfil the aforementioned responsibilities in the perforated circuit board. The only use currently is to house the battery and the wall adaptor input circuit to power the microcontroller unit.

IV. Software Design

A. Embedded software

The software installed on the ESP32-CAM was developed using a hybrid of programs with the C language and Wiring language for Arduino. Development was done mostly in the C language since that was what the available documentation was written for. This was required to set up the parallel camera interface with the ESP32 to use the OV2640 image sensor. The remaining programming was done in the Wiring language which had

available documentation when setting up the asynchronous web server for the client application.

B. Python Application

Using the Kivy framework for Python, we were able to develop a software solution that would be compatible with any Mac, Windows, iOS and Android that would allow control over the microcontroller's functions for the semi-automated SPR sensor such as reading the input voltage of specific pins that would give the user an estimated battery life that remain for the LiPo battery if one is plugged in.

The application will guide the user through an SPR experiment and instruct them how to use the Thorlabs rotation platform to achieve SPR with a view of the camera input projected onto the screen. The software can monitor the status of the camera sensor and optimize for a consistent capture rate to ensure a smooth transition when obtaining SPR. The application will process the images into what we defined as perceived brightness which uses a histogram type approach when finding the intensity of the incoming beam and will graph this date over time.

The original vision was to have a fully automated SPR device but with time constraints and the impact on manufacturing due to COVID-19 it was not completed as such. Our final version of the SPR system uses a Thorlabs brand rotation platform powered by a controller unit that made fully automated sensing impossible. The final version of the software still contains the functionality to have the microcontroller turn the power on or off for the originally used laser diode plus the use of a stepper motor to replace the rotation platform.

V. Results

To first confirm that surface plasmon excitation is occurring, an experiment was performed in free space where the power of the light is monitored at different angular increments. The information collected was compiled into Excel to confirm the existence of surface plasmon resonance on the surface of the gold film. The power readings were collected at 0.5° increments starting at 38° until reaching 50°. A simulation of the surface plasmon resonance curve was generated using Winspall and superimposed with the collected power readings, which can be seen in Figure 5. The measured power readings were normalized to match the reflectivity range of the light from 0 to 1, with 1 being the maximum output power of the laser after the polarizing beamsplitter and 0 being no power observed.

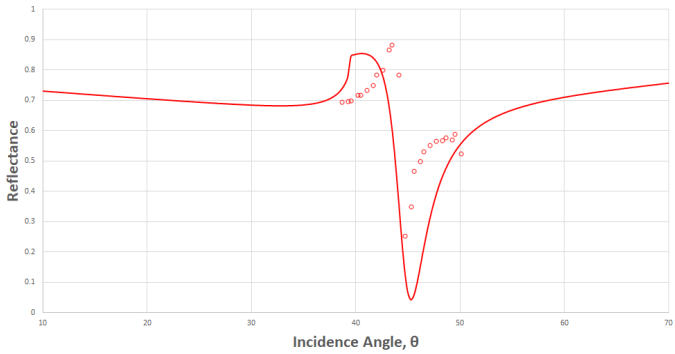

Figure 5. Simulation vs. experimental: reflectance as a function of incidence angle measured. Solid line corresponds to simulated data, open circles correspond to experimental data.

Comparing the simulation data with that of the experiment, the angle where SPR occurred for the experiment closely resembled that of the simulation. The simulation observed the critical angle at 39.5° and the experimental critical angle was found at 41°, giving a margin of error of 3.7%. The maximum drop in intensity in the experiment was found at 44.5° while the maximum drop in intensity simulated was found at 45°. This gives us a percentage accuracy of 98.8%.

The next step was to confirm our experimental results could be detected by our CMOS sensor camera and the designed software. To do this, the rotation stage was set at 44° and rotated at a velocity of 0.5° per second until reaching 48°. The intensity of the reflected beam was captured by the camera and the intensity profile of each image processed and displayed graphically using the software application, which can be seen in Figure 6.

The change in intensity displayed on the software follows closely to that observed experimentally using an optical power meter. The experiment using our software was tested multiple times using different gold SPR chips, and the angle and drop in intensity observed remained relatively consistent for each experiment. This showed that our device can easily repeat experiments even with different SPR chips applied to the sensing location.

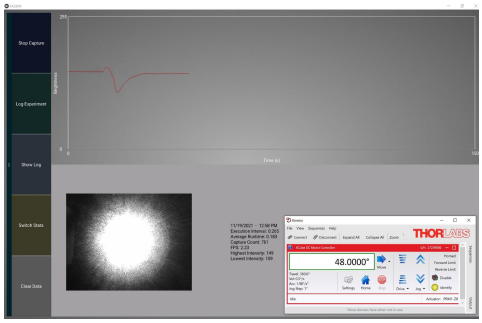

Figure 6. SASSPR software displaying graphically the SPR curve in air as Reflectance vs. Time.

Next, distilled water was added into the sensor chamber at the SPR angle found in air. Distilled water was chosen for a number of factors. The primary reason was distilled water having a refractive index of 1.324, which is greater than that of air. Choosing a dielectric material with a higher refractive index allows us to demonstrate our device as it detects shifts in the resonance angle when increasing the refractive index of the material in contact with the interface of the gold film. Distilled water was also chosen due to the distillation process removing the electrical charge from atoms and molecules in the water, thus providing more accurate results in laboratory settings. Once the distilled water was added to the sensor chamber, the intensity of the reflected light immediately increased. This indicated that our SPR angle had shifted due to a change in the refractive index observed on the surface of the gold film. This portion of the experiment proved our device could monitor changes in the resonance angle using intensity modulation.

VI. Conclusion

We have presented a device that allows for surface plasmon resonance on thin metal films to be observed and recorded. The optical components ensure that the proper polarization, wavelength, and alignment of our laser source is correct for phase matching to occur between the wave of our incident light and the wave of the surface plasmons on the metal film, while the electrical and computer components ensure our detector properly captures the necessary intensity changes observed and represents them in a user-friendly software application. We have also demonstrated that the surface of the metal film is highly sensitive to changes to its refractive index, which was confirmed when distilled water was introduced into the sensing chamber and an increase in intensity was detected at the angle where surface plasmon excitation was previously seen. Our device could be later improved to allow for the software application to fully control the laser source and motorized rotation stage for more precise measurements of the exact angle of surface plasmon resonance to be determined. Nevertheless, we have presented a device that can detect and display surface plasmon excitation and monitor shifts in the resonance angle through intensity modulation.

Biographies

Robin Howell is currently a senior at the University of Central Florida and will receive his Bachelor's of Science in Photonic Science and Engineering in December of 2021. He plans to continue his education and pursue his Masters in Optics and Photonics.

Robert Ballentine will complete his Bachelor's of Science in Photonic Science and Engineering in December 2021. He plans on working in industry while simultaneously pursuing his masters in Optics and Photonics to specialize in Laser Sciences in Fall 2022.

James Henderson will receive his Bachelor's of Science in Computer Engineering in December of 2021 with a minor in Physics and Psychology. He plans on starting the Master of Science program in Modeling and Simulation in Spring 2022.

References

[1] Kik, P., SP excitation and detection, in OSE 6650: Optical Properties of Nanosctructured Materials. 2021: University of Central Florida.

[2] Raether H. (1988) Surface plasmons on smooth surfaces. In: Surface Plasmons on Smooth and Rough Surfaces and on Gratings. Springer Tracts in Modern Physics, vol 111. Springer,Berlin,Heidelberg.https://doi.org/10.1007/BFb0048319